



Cite this: *Phys. Chem. Chem. Phys.*,
2025, 27, 18760

The role of oxygen in the synthesis of the Mo_2CT_x MXene from the $\text{Mo}_2\text{Ga}_2\text{C}$ MAX phase

José D. Gouveia *^a and José R. B. Gomes *^b

MAX phases are layered materials that have been known for over 60 years and MXenes are their metaphorical children, a family of two-dimensional (2D) materials that appeared in 2011. MXenes are often synthesised by etching out the layers of the A element of their parent MAX phases. The remaining 2D MXene layers are very reactive and spontaneously become covered by a layer called the surface termination. The Mo_2C MXene was first synthesised in 2015, by using hydrofluoric acid to remove the Ga layers from the $\text{Mo}_2\text{Ga}_2\text{C}$ MAX phase, and its surface termination was determined to be mostly composed by O groups. While the layers of Mo and C in $\text{Mo}_2\text{Ga}_2\text{C}$ are arranged in a face-centred cubic manner, those of Mo_2C prefer a hexagonal close-packed stacking. This implies that, at some point during the etching process, a phase transition should occur because of the replacement of Ga by O. Herein, we employ density-functional theory calculations to analyse the thermodynamics of this process by assessing the stability of the two stacking phases of the $\text{Mo}_2\text{Ga}_2\text{C}$ MAX phase, as the Ga atoms are gradually replaced by O ones. Among other results, we identify the preferred locations of O and F atoms in the $\text{Mo}_2\text{Ga}_2\text{C}$ lattice, propose a possible explanation for the greater presence of O atoms over F ones on the surface of as-synthesised Mo_2C MXenes, evaluate the interaction between O atoms in $\text{Mo}_2\text{Ga}_2\text{C}$ crystals, estimate the energy of Ga–Ga bonds, and lastly, show that the relative stability of the two stacking phases of $\text{Mo}_2\text{Ga}_2\text{C}$ is reversed when approximately half of the Ga content is replaced by O.

Received 17th June 2025,
Accepted 11th August 2025

DOI: 10.1039/d5cp02315g

rsc.li/pccp

Introduction

MAX phases and MXenes are two families of layered materials that are inexorably connected. The stoichiometry of the former (three-dimensional solids) can traditionally be written as $\text{M}_{n+1}\text{AX}_n$ ($n = 1$ to 4), where M is an early transition metal, A is an element usually from groups 13 or 14 of the Periodic Table of the Elements, and X is carbon and/or nitrogen.¹ Structurally, $n + 1$ layers of the M element, intercalated by n layers of the X element in a face-centred cubic (FCC) arrangement (distorted XM_6 octahedra), are separated by single flat layers of the A element. MXenes are the two-dimensional (2D) derivatives of MAX phases, obtained by etching out the A layers of their parent structures, and retaining only the M_{n+1}X_n scaffold.^{2,3} The outermost layers of these 2D materials comprise M atoms and are very reactive, so that the stoichiometry of as-synthesised MXenes is in fact $\text{M}_{n+1}\text{X}_n\text{T}_x$, where T is the surface termination, whose composition (most commonly –O,

–F and –OH groups) depends on the synthesis conditions. The first MXene, Ti_3C_2 , was synthesised from the Ti_3AlC_2 MAX phase, from which the Al atoms were removed in the form of aluminium fluoride (AlF_3).²

While MAX phases have been known for over 60 years⁴ and more than 300 different ones have been produced,¹ accounting for multiple n and M, A and X element combinations, MXenes are a relatively new family, with only a few tens of members realized, although hundreds have been predicted to be stable.³ MXenes display high electrical conductivity, mechanical robustness, and tuneability inherited from MAX phases. Being 2D, MXenes find application in sensing,^{5–8} catalysis,^{9–12} hydrogen storage,^{13–15} electronics and photonics,¹⁶ among others.^{17–19}

Since MXenes are mostly obtained from MAX phases, the interest in synthesizing new MXenes has in turn motivated the synthesis of novel MAX phases, as may have happened in the search for the Mo_2C MXene. The Mo_2GaC MAX phase was first reported in 1967,²⁰ but the removal of the Ga layers from it to form the Mo_2C MXene has proven very challenging thus far. However, in 2015, four years after the introduction of MXenes, a new layered material, with stoichiometry $\text{Mo}_2\text{Ga}_2\text{C}$, was discovered.²¹ This was assumed to be the first of a new family, but some authors simply call it a double A-layer MAX phase. Since then, at least 10 different double A-layer MAX phases,

^a CICECO-Aveiro Institute of Materials, Department of Physics, University of Aveiro, Campus Universitário de Santiago, 3810-193 Aveiro, Portugal.

E-mail: gouveia@ua.pt

^b CICECO-Aveiro Institute of Materials, Department of Chemistry, University of Aveiro, Campus Universitário de Santiago, 3810-193 Aveiro, Portugal.

E-mail: jrgomes@ua.pt



with stoichiometries M_2A_2X and $M_3A_2X_2$, have been reported, but Mo_2Ga_2C is the only one that was realized by direct synthesis, rather than by modifying existing MAX phases.¹ The Mo_2Ga_2C MAX phase is an unusual one, not only for having two layers of the A element per formula unit, but also for the fact that these two layers sit exactly on top of each other, instead of a close-packed fashion.²¹ In the same year that Mo_2Ga_2C was discovered, the same group was finally able to synthesize the Mo_2C MXene,²² representing both the first Mo-based MXene to be made and the first MXene to be derived from a non-Al MAX phase. The Mo_2C MXene was attained in the most usual way, *i.e.*, by immersing the parent Mo_2Ga_2C MAX phase in 50% concentrated hydrofluoric acid for a few hours at 50 °C, resulting in the effective removal of almost all the Ga content. In the same work, this procedure was also attempted on Mo_2Gac MAX phase samples, but unsuccessfully. For this reason, since then, all subsequent syntheses of the Mo_2C MXene are performed from the double A-layer MAX phase, Mo_2Ga_2C , even when employing hydrothermal routes involving 24-hour etching with $LiF + HCl$, $NaF/KF + HCl$, or $NH_4F + HCl$ solutions at temperatures ranging from 140 to 180 °C.²³ The as-synthesized Mo_2CT_x MXene had an approximate Mo:Ga:O:F content of 50:5:40:5.²² In other words, it contained little Ga, as intended, and exhibited a surface termination dominated by oxygen atoms.

The transition from the Mo_2Ga_2C MAX phase to the Mo_2CT_x MXene is a curious one, since the Mo_2C atomic layers in the MAX phase are known to be arranged in an FCC manner (also known as ABC stacking),^{24,25} whereas the Mo_2CT_x MXenes have their atomic layers arranged in a hexagonal close-packed structure (also known as ABA stacking), regardless of the composition of the surface termination.^{12,26,27} This raises several questions. For example, is the Mo_2Ga_2C MAX phase (*meta*)stable in an ABA stacking phase? Can the replacement of Ga atoms by O ones drive the transition from the ABC to the ABA atomic layer stacking? In this work, we answer these questions by performing density-functional theory (DFT) calculations to study the interaction of the Mo_2Ga_2C MAX phase with oxygen and fluorine atoms, and by comparing the relative stability of the ABC and ABA stacking sequences in Mo_2Ga_2C MAX phase models with varying degrees of Ga-to-O substitution.

Computational method

We performed spin-polarized DFT calculations using the VASP code²⁸ and the PBE exchange–correlation functional, within the generalized gradient approximation.²⁹ The explicitly treated electrons were Mo: 4p⁶ 4d⁵ 5s¹, Ga: 3d¹⁰ 4s² 4p¹, C: 2s² 2p², and O: 2s² 2p⁴. The remaining core electrons were implicitly considered through the projector augmented-wave method.³⁰ Given that we are studying the transition from a three-dimensional MAX phase to two-dimensional MXene layers, it is expected that van der Waals interactions become relevant, at least between neighbouring MXene surfaces, so we investigated how some of our results change when D3 dispersion corrections³¹ are

included in the calculations. The PBE(-D3) approach is employed in this work to ensure consistency and enable direct comparison with values reported in the literature, as it is the most commonly used functional in computational studies of MXenes.³² Given that both the Mo_2Ga_2C MAX phase and the Mo_2C MXene are known to exhibit metallic behavior, the use of higher-level functionals, such as hybrid approaches, would not alter their classification as metals, while other calculated properties would likely remain largely unchanged, though at significantly increased computational cost. Recent comparative studies of dispersion-corrected functionals, including PBE-TS, PBE-D2, PBE-D3, vdW-DF, vdW-DF2, optB88-vdW, and optB86b-vdW approaches, have identified PBE-D3 as the most accurate for computing out-of-plane lattice parameters,³³ and binding energies³⁴ in related transition-metal dichalcogenides. These findings further support the choice of computational methodology adopted in this work.

In our calculations, we used periodic models of different sizes (Fig. 1) and different simulation parameters for different purposes. We performed three types of calculations. In a first stage (1), we considered single unit cells of Mo_2Ga_2C or Mo_2CO_2 , with ABC or ABA atomic layer stacking, and calculated their lattice parameters, relative stability and electronic band diagrams. Then, in the second stage (2), we studied the interaction between Mo_2Ga_2C and O or F atoms, as well as the interaction between substitutional O atoms in Mo_2Ga_2C . In the last stage (3), we investigated how the relative stability of ABC- and ABA-stacked Mo_2Ga_2C changes with an increasing amount of substitutional O. The simulation parameters resulted from preliminary tests ensuring that relative energies are converged within less than 1 meV per atom and maximizing accuracy/efficiency trade-off, and are the following:

(1) Unit cell calculations were conducted to obtain lattice parameters and electronic band diagrams of pristine Mo_2Ga_2C and Mo_2CO_2 . Each model of a unit cell contains two formula units and D3 dispersion corrections were included in the Mo_2CO_2 MXene calculations. A large energy cutoff of 550 eV was employed, and tight atomic and electronic relaxation criteria were adopted as well, namely 5 meV Å⁻¹ and 1 μeV, respectively. The Brillouin zones were sampled using Γ -centred 15 × 15 × 3 grids of special k points for the calculations of lattice parameters.³⁵ The energy band diagrams were calculated using an explicit list of k points interpolated between high-symmetry points of the Brillouin zone of each material.

(2) The analysis of point defects in Mo_2Ga_2C requires the use of larger models to partially screen unwanted interaction between periodic copies of each defect. Thus, we built supercells made of 4 × 4 × 1 unit cells of Mo_2Ga_2C , ensuring a separation of at least 12 Å between the periodic copies. Here, we used an energy cutoff of 415 eV, and atomic and electronic relaxation criteria of 0.01 eV Å⁻¹ and 0.01 meV, respectively. A Γ -centred grid with 3 × 3 × 3 special k points was used to sample the Brillouin zones.³⁵

(3) The assessment of how the relative stability of ABC- and ABA-stacked Mo_2Ga_2C is modified as the concentration of substitutional O increases was done on models comprising



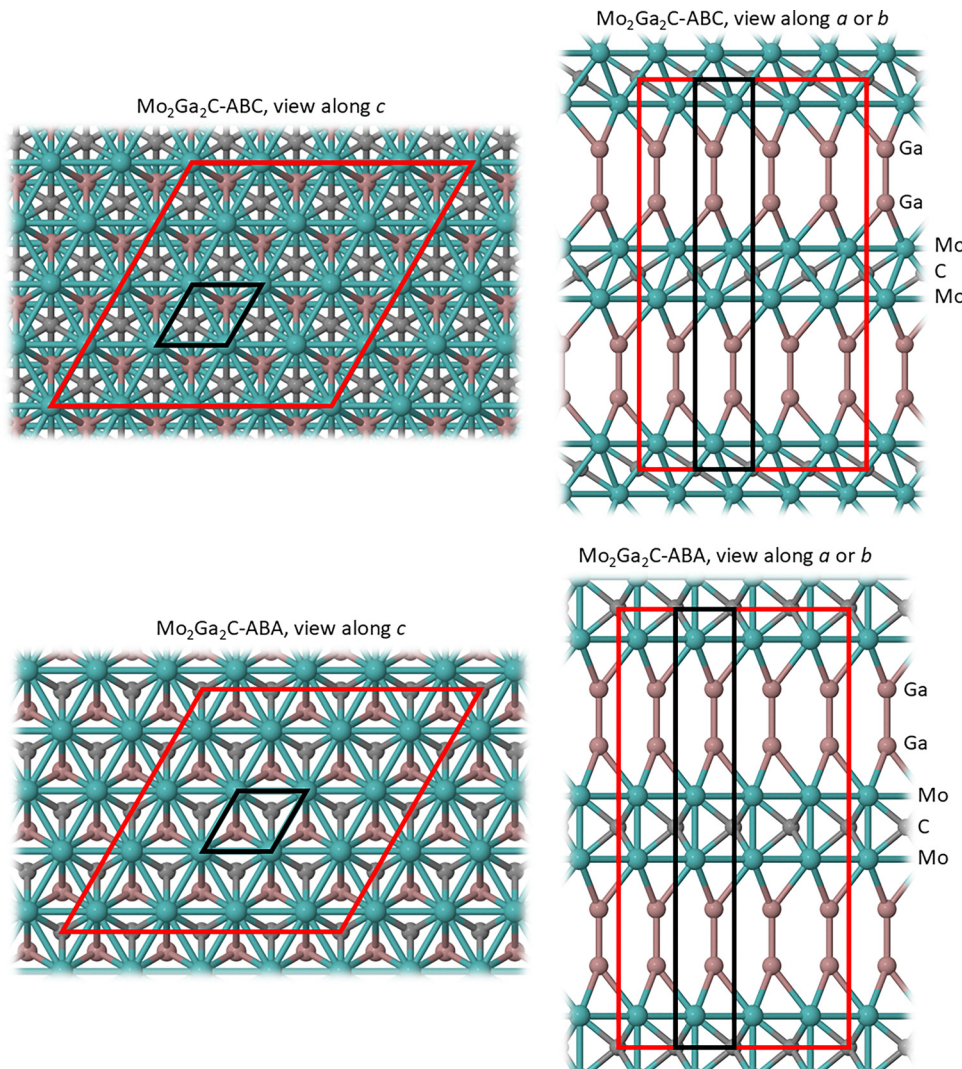


Fig. 1 Views of models of a unit cell (black lines) and a 4×4 supercell (red lines) of $\text{Mo}_2\text{Ga}_2\text{C}$ used in this work, with ABC (ABA) stacking shown in the top (bottom) panels. The models of the Mo_2CO_2 MXene with ABC and ABA atomic layer stacking are analogous to the ones of $\text{Mo}_2\text{Ga}_2\text{C}$ with the same stacking, with the Ga atoms replaced by O ones. The panels on the left show views along the c lattice vector, whereas the ones on the right show views along the a or b lattice vectors (the a and b directions are equivalent). Colour code for the spheres: Mo in cyan, Ga in pink, C in grey.

$2 \times 2 \times 1$ unit cells of $\text{Mo}_2\text{Ga}_2\text{C}$. Furthermore, the calculations were done separately in three ways to enable comparison of the results from each procedure: (i) with the PBE functional (without D3 corrections) and a fixed supercell size, (ii) with D3 corrections and fixed supercell size, and (iii) with D3 corrections and optimization of the supercell size for each O concentration. Here, we used the same energy cutoff and convergence criteria as in the study of point defects, and a Γ -centred grid with $7 \times 7 \times 3$ special k points was used to sample the Brillouin zones.³⁵

The formation energies, E_{form} , of defects involving a single O or F atoms in $\text{Mo}_2\text{Ga}_2\text{C}$ were calculated as

$$E_{\text{form}} = E_{\text{defect}} - E_{\text{pristine}} + E_{\text{removed}} - E_{\text{added}} \quad (1)$$

Here, E_{defect} and E_{pristine} are the total energies of a supercell containing $4 \times 4 \times 1$ unit cells of defective or pristine $\text{Mo}_2\text{Ga}_2\text{C}$, respectively. The quantities E_{removed} and E_{added} are the energies of

the atoms that were removed or added to create the defect, respectively. In the case of interstitial defects, E_{removed} is zero. The energies of a single Ga, C or O atom were calculated as the total energy per atom of a Ga bulk orthorhombic unit cell, a diamond unit cell, or an O_2 molecule. The energy of an F atom was calculated by subtracting half the energy of an H_2 molecule from that of an HF one, because the process of etching out the Ga layers from $\text{Mo}_2\text{Ga}_2\text{C}$ uses HF as a reagent. The energies of the isolated molecules were obtained by optimizing them in an asymmetric box with dimensions $10 \times 11 \times 12 \text{ \AA}$, employing Γ -point sampling.

Results and discussion

Pristine $\text{Mo}_2\text{Ga}_2\text{C}$ MAX phase and Mo_2CO_2 MXene

The structure of $\text{Mo}_2\text{Ga}_2\text{C}$ (with the usual ABC stacking of its atomic layers) can be described as ABC-stacked Mo_2C MXenes



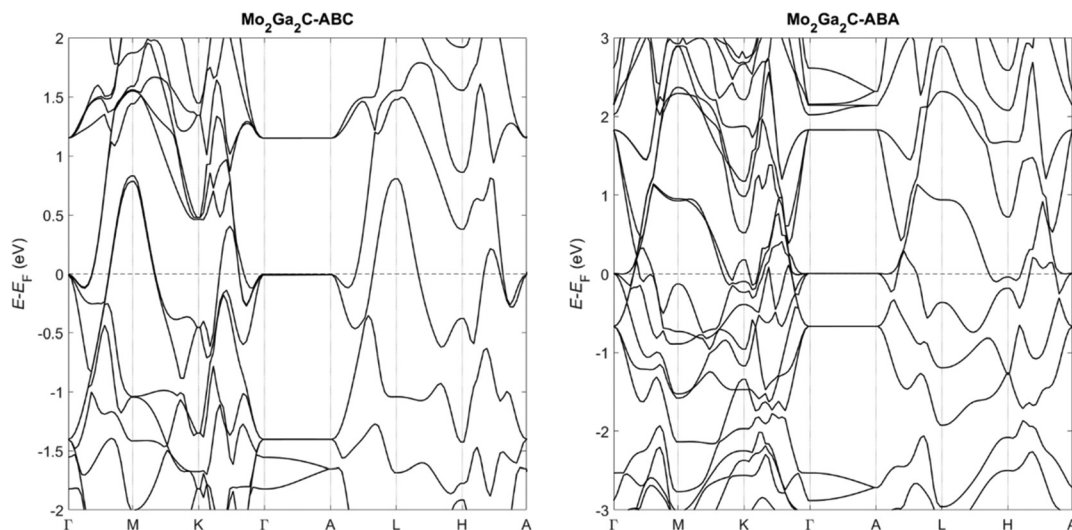


Fig. 2 Calculated band structure of $\text{Mo}_2\text{Ga}_2\text{C}$. The horizontal dashed line lies at the Fermi energy.

connected to each other by pairs of Ga atoms, in which the Ga–Ga bonds are perpendicular to the basal plane. The $\text{Mo}_2\text{Ga}_2\text{C}$ -ABA can be described in an analogous way, but the Mo_2C sections are aligned in an ABA fashion instead. Several relative alignments of the Mo_2C layers and of the Ga layers along the direction of the c lattice vector are possible, and the thermodynamic stability of all of them was studied, leading to the conclusion that the most stable one is as shown in Fig. 1. The unit cell of $\text{Mo}_2\text{Ga}_2\text{C}$ -ABA seen in Fig. 1 is in fact composed of two primitive cells on top of each other, but we chose to study it this way to enable a more direct comparison with $\text{Mo}_2\text{Ga}_2\text{C}$ -ABC, upon consideration of the same number of atoms of each species and more similar box volumes.

The calculated band diagrams of $\text{Mo}_2\text{Ga}_2\text{C}$ -ABC and $\text{Mo}_2\text{Ga}_2\text{C}$ -ABA are shown in Fig. 2. The band structures of both carbides indicate that they display metallic nature. In the case of $\text{Mo}_2\text{Ga}_2\text{C}$ -ABC, this is in consonance with the results of ref. 36, where a visually identical band structure of $\text{Mo}_2\text{Ga}_2\text{C}$ (ABC) was predicted.

Table 1 contains the calculated lattice parameters of the $\text{Mo}_2\text{Ga}_2\text{C}$ MAX phase with either atomic layer stacking, and of the same materials when all Ga atoms are replaced by O ones, generating a $\text{Mo}_2\text{O}_2\text{C}$ “MOX phase”. The lattice parameters of $\text{Mo}_2\text{Ga}_2\text{C}$ -ABC ($a = 3.07 \text{ \AA}$ and $c = 18.12 \text{ \AA}$) are within 1% of the ones measured in ref. 21 ($a = 3.05 \text{ \AA}$ and $c = 18.19 \text{ \AA}$), where the first synthesis of this MAX phase was reported. Notice that

the lattice parameters a and c of $\text{Mo}_2\text{Ga}_2\text{C}$ -ABA deviate from the experimental ones by -4% and $+6\%$, respectively. In contrast, the calculated a of $\text{Mo}_2\text{O}_2\text{C}$ -ABA (2.89 \AA), which resembles an ABA-stacked Mo_2CO_2 MXene, is in close agreement with the same parameter measured experimentally for the Mo_2CT_x MXene in ref. 27 (2.86 \AA), while the same parameter calculated for the MXene-like $\text{Mo}_2\text{O}_2\text{C}$ -ABC (2.96 \AA) differs from the experimental one by 4%. These results support the fact that synthesised $\text{Mo}_2\text{Ga}_2\text{C}$ MAX phases display an ABC atomic layer stacking in its Mo_2C layers, assumed in the literature,^{24,25} while the Mo_2C MXenes produced by removing the Ga layers of $\text{Mo}_2\text{Ga}_2\text{C}$ have their atomic layers stacked in an ABA (hexagonal close-packed) arrangement.¹² The ABC stacking of experimentally obtained $\text{Mo}_2\text{Ga}_2\text{C}$ MAX phases is further supported by our calculated relative thermodynamic stability of the $\text{Mo}_2\text{Ga}_2\text{C}$ -ABC and ABA models, which is 1.05 eV per unit cell in favour of the ABC-stacked model. This value changes by less than 0.1 eV with the inclusion of D3 dispersion corrections in the calculations.

If one includes D3 dispersion corrections to calculate the values in Table 1, the a parameters are left unchanged, and the c ones are reduced by 1 \AA for $\text{Mo}_2\text{O}_2\text{C}$ only. As expected, the dispersion corrections have a greater effect on results relative to $\text{Mo}_2\text{O}_2\text{C}$. Nevertheless, the calculated c lattice constants of $\text{Mo}_2\text{O}_2\text{C}$ are not relevant because, experimentally, the Ga-etching out of $\text{Mo}_2\text{Ga}_2\text{C}$ MAX phases originates MXenes in a solution with concomitant intercalation of solvent molecules and of other species present in the reaction medium (see, for example, Fig. 2 in ref. 37), so the measured c parameters of Mo_2CT_x are naturally much larger (20.5 \AA and 24.7 \AA in ref. 27 and 22, for example) than the ones predicted by calculations in vacuum.

From the data shown in Table 1, one additionally infers that the replacement of Ga atoms with O ones reduces the values of all the lattice parameters of the $\text{Mo}_2\text{Ga}_2\text{C}$ MAX phase, which was expected, given the reduced size of O atoms when

Table 1 Calculated lattice parameters of $\text{Mo}_2\text{Ga}_2\text{C}$. The notation $\text{Mo}_2\text{O}_2\text{C}$ represents $\text{Mo}_2\text{Ga}_2\text{C}$ models in which all Ga atoms were replaced by O ones, and the positions and cell size reoptimized. The values shown are for calculations without D3 dispersion corrections

Material	$a = b (\text{\AA})$	$c (\text{\AA})$
$\text{Mo}_2\text{Ga}_2\text{C}$ -ABC	3.07	18.12
$\text{Mo}_2\text{Ga}_2\text{C}$ -ABA	2.93	19.36
$\text{Mo}_2\text{O}_2\text{C}$ -ABC	2.96	16.61
$\text{Mo}_2\text{O}_2\text{C}$ -ABA	2.89	17.18



compared with that of Ga atoms. However, even when adding dispersion corrections in the calculations, which reduce the *c* lattice constants of $\text{Mo}_2\text{O}_2\text{C}$, the distance between nearest O atoms is greater than that the bond length of the Ga pairs. On $\text{Mo}_2\text{Ga}_2\text{C}$ -ABC, the Ga-Ga distance was estimated at 2.49 Å, which increases to an O-O distance of 2.73 Å on $\text{Mo}_2\text{O}_2\text{C}$ -ABC (with D3). Likewise, on $\text{Mo}_2\text{Ga}_2\text{C}$ -ABA, the Ga-Ga distance was estimated at 2.51 Å, and increases to an O-O distance of 2.79 Å on $\text{Mo}_2\text{O}_2\text{C}$ -ABA (with D3). This prompted us to calculate the binding energy of the $\text{Mo}_2\text{O}_2\text{C}$, *i.e.*, the energy per formula unit required to separate the $\text{Mo}_2\text{O}_2\text{C}$ MOX phase into individual Mo_2CO_2 MXene sheets, which can be calculated as half the energetic difference between a $\text{Mo}_2\text{O}_2\text{C}$ unit cell and two Mo_2CO_2 unit cells. The calculated binding energies are -0.23 and -0.22 eV for the ABC- and ABA-stacked models, suggesting that $\text{Mo}_2\text{O}_2\text{C}$ is in fact a van der Waals solid, formed by weakly interacting two-dimensional Mo_2CO_2 MXene layers. For comparison, the calculated binding energy per unit cell of the (three-dimensional) $\text{Mo}_2\text{Ga}_2\text{C}$ with respect to two (two-dimensional) Mo_2CGa_2 MXene-like sheets is -1.14 and -1.55 eV for the for the ABA- and ABC-stacked surfaces, respectively. Hence, the binding of $\text{Mo}_2\text{Ga}_2\text{C}$ is stronger than that of Mo_2CO_2 , despite the larger *c* lattice parameter of the former. This also indicates that the decrease in this lattice parameter when transitioning from the MAX phase to the MXene is not due to stronger interaction between adjacent sheets, but instead can simply be due to the smaller size of O atoms when compared to Ga ones.

The coordinates of optimized $2 \times 2 \times 1$ supercells of $\text{Mo}_2\text{Ga}_2\text{C}$ and $\text{Mo}_2\text{O}_2\text{C}$, with ABC and ABA atomic layer stacking, are included in the SI.

O- and F-related point defects in the $\text{Mo}_2\text{Ga}_2\text{C}$ MAX phase

Since the synthesis method of the Mo_2CT_x MXene involves the use of hydrofluoric acid and the resulting MXene is functionalized mostly by O groups with some F groups,^{22,27} we investigated the interaction of O and F atoms with $\text{Mo}_2\text{Ga}_2\text{C}$ (with ABC atomic layer stacking, since we have established that this is the most accurate model). Three kinds of defects were analysed for each atom: interstitials (O_{int} or F_{int}), Ga substitution (O_{Ga} or F_{Ga}), and C substitution (O_{C} or F_{C}). We considered Ga

substitution because it is expected to occur naturally during the Ga-etching process, and C substitution because certain MAX phases are known to incorporate oxygen into their carbon sublattices, a characteristic that can be passed onto their corresponding A-element-etched MXene derivatives.^{38–41} The interstitial O or F positions that were analysed involve bonding with at least one Ga atom of $\text{Mo}_2\text{Ga}_2\text{C}$, as was done, for example, in ref. 42 and 43 for self-interstitials and O and H interstitials in the Ti_2AlN MAX phase. Therefore, five inequivalent interstitial sites were considered for O or F, as shown in Fig. 3. Three of these coincide with the interstitial sites in MAX phases with one atom of the A element per formula unit: the tetrahedral Ga_3Mo (*i.e.*, O or F is inside a tetrahedron formed by three Ga atoms and one Mo atom) and GaMo_3 sites, and the octahedral Ga_3Mo_3 site. The other two interstitial sites are considered in this work for the first time because they are exclusive to MAX phases with more than one atom of the A element per formula unit, since they are located inside the triangular prisms formed by six Ga atoms.

The formation energies of each of these defects are given in Table 2. Note that using different species as reference can yield different formation energies. For example, in this work, the energy of a single F atom is $E(\text{F}) = E(\text{HF}) - E(\text{H}_2)/2$, but we could have simply done $E(\text{F}) = E(\text{F}_2)/2$, and this would lead to lower formation energies.⁴⁴ However, the predicted relative thermodynamic stability of the F-related defects would be the same. Thus, we conclude that, for both O- and F-related defects, the ones with the lowest formation energies are Ga substitutions, followed by O or F interstitials. In Table 2, only four rows of interstitial defects are shown because O_{int} and F_{int} at the $\text{Ga}_6(\text{Mo})$ site are not stable and, upon relaxation, become Ga_3Mo . Interstitial oxygen atoms are indeed present in some MAX phases, such as Ti_2AlN .⁴³ The formation energy of F_{C} is considerably higher than any other value in Table 2, which might be a reason why, although HF is used to produce MXenes, oxycarbide and oxynitride MXenes have been observed, while no fluorocarbide or fluoronitride ones have been reported.

Structurally, O_{Ga} and F_{Ga} are significantly different. As shown in Fig. 4, a substitutional O binds to three Mo atoms of the nearest Mo_2C slab, and its position relative to the nearest Mo_2C slab is analogous to the FCC-like site where surface

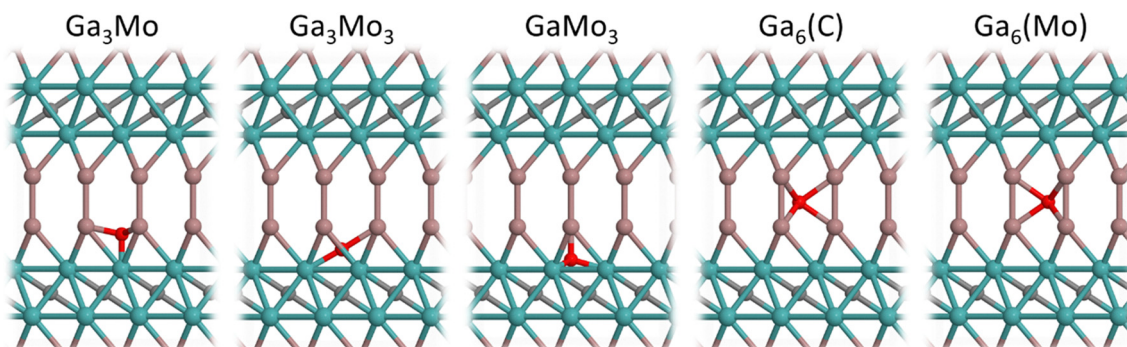


Fig. 3 Possible interstitial sites for O or F (only O shown here). Colour code for the spheres: Mo in cyan, Ga in pink, C in grey, O in red.



Table 2 Formation energies (E_{form}) of O- and F-related single-site point defects in the $\text{Mo}_2\text{Ga}_2\text{C}$ MAX phase. The lowest formation energy among the defects related to each atom is written in bold font

O defects	F defects		
Site	E_{form} (eV)	Site	E_{form} (eV)
$\text{O}_{\text{int}}\text{Ga}_3\text{Mo}$	-2.01	$\text{F}_{\text{int}}\text{Ga}_3\text{Mo}$	+0.54
$\text{O}_{\text{int}}\text{Ga}_3\text{Mo}_3$	-1.00	$\text{F}_{\text{int}}\text{Ga}_3\text{Mo}_3$	+1.99
$\text{O}_{\text{int}}\text{GaMo}_3$	-0.37	$\text{F}_{\text{int}}\text{GaMo}_3$	+3.37
$\text{O}_{\text{int}}\text{Ga}_6(\text{C})$	-0.14	$\text{F}_{\text{int}}\text{Ga}_6(\text{C})$	+1.60
O_{Ga}	-2.65	F_{Ga}	-0.68
O_{C}	-0.74	F_{C}	+4.14

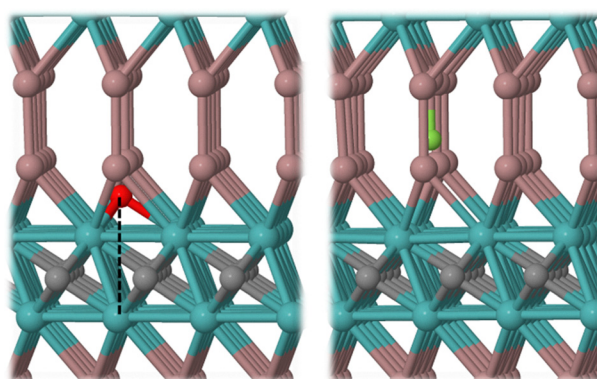


Fig. 4 Structures of the Ga-substitutional O (left) and Ga-substitutional F (right) defects in $\text{Mo}_2\text{Ga}_2\text{C}$. The dashed line shows the vertical alignment between the O atom and the farthest Mo atom of the nearest Mo_2C slab. Colour code for the spheres: Mo in cyan, Ga in pink, C in grey, O in red, F in green.

terminations are preferably located on most MXenes, *i.e.*, a hollow surface site above an atom of the M element.^{8,45} The O_{Ga} atom is substantially closer (downwards in Fig. 4, by 1.1 Å) to the Mo_2C slab than the Ga atom was. In turn, a substitutional F_{Ga} atom in the $\text{Mo}_2\text{Ga}_2\text{C}$ lattice prefers to move 0.8 Å away (upwards in Fig. 4) from the nearest Mo_2C planes and bind to the other Ga atom of the Ga–Ga pair. Possibly, this is related to HF being so successful in breaking Ga–Mo bonds and etching out the Ga layers, to the more prominent occurrence of an O surface termination (80%), when compared to F (10%), in the synthesised Mo_2C MXene reported in ref. 22. Furthermore, the fact that substitutional F atoms bind to Ga atoms in $\text{Mo}_2\text{Ga}_2\text{C}$, at least during the initial stages of Ga etching, suggests that Ga atoms may be removed in the form of an incipient gallium fluoride species, such as trigonal GaF_3 , the most stable gallium fluoride, in analogy with the aluminium fluoride (AlF_3) that forms when synthesising Ti_3C_2 from the Ti_3AlC_2 MAX phase.

According to our calculations, many of the defects studied here attract each other, as illustrated in Fig. 5. This is true for substitutional O atoms, for which the energetic difference between two O atoms replacing two Ga atoms of the same Ga–Ga pair, and replacing two Ga atoms far from each other, is 1.21 eV in favour of the former. This makes sense from the point of view of chemical bonds: replacing a Ga–Ga pair by an O–O pair requires breaking six Ga–Mo bonds and one Ga–Ga

one, while replacing two Ga atoms by two O atoms far from each other requires breaking six Ga–Mo bonds and two Ga–Ga ones, *i.e.*, one more Ga–Ga bond. We verified this by comparing the energy of two Ga vacancies far from each other, with that of a Ga–Ga pair vacancy, and found the latter is more stable by 1.20 eV, implying that Ga vacancies attract each other as well. Equivalently, this energy can be used as an estimate of the Ga–Ga bond energy in $\text{Mo}_2\text{Ga}_2\text{C}$. The 1.20 eV value is within the calculated binding energies per unit cell of ABA- and ABC-stacked surfaces of $\text{Mo}_2\text{Ga}_2\text{C}$ reported above. Curiously, we found that pairs of substitutional O atoms are also thermodynamically more stable when next to each other. All these results suggest a cascading effect when etching out the Ga layers of $\text{Mo}_2\text{Ga}_2\text{C}$, wherein regions of the material adjacent to where Ga atoms have been replaced by O ones are more prone to have their Ga content replaced by O as well. Hence, as Ga atoms are etched out of the $\text{Mo}_2\text{Ga}_2\text{C}$ MAX phase, O atoms from O-containing species in solution occupy neighbouring Ga sites, serving as the surface termination of the Mo_2C MXene that is eventually formed.

Although the Mo_2C MXene has been synthesised numerous times since the discovery of the $\text{Mo}_2\text{Ga}_2\text{C}$ MAX phase,²² attempts to obtain it from the Mo_2GaC MAX phase have proved elusive. For comparison, we analysed the structure of a Ga-substituting O atom in Mo_2GaC , using the same simulation parameters as for $\text{Mo}_2\text{Ga}_2\text{C}$, but with a model containing only one Ga atomic layer between each pair of Mo_2C slabs. As shown in Fig. S1, we observed that the most stable position of O_{Ga} in Mo_2GaC is amid the Ga layer, bonded to two Ga atoms, contrasting with the same defect in $\text{Mo}_2\text{Ga}_2\text{C}$, in which O_{Ga} binds to the three nearest Mo atoms. It is well known that MXenes are enormously stabilized when their surfaces are functionalized. Therefore, it is possible that, in order to produce the Mo_2C MXene (and possibly other MXenes) from a MAX phase, having O atoms serving as the surface termination of the MXene is a requirement to stabilize the new 2D material and produce the cascading effect mentioned in the previous paragraph.

Atomic layer stacking stability in the $\text{Mo}_2\text{Ga}_2\text{C}$ MAX phase with increasing O content

After having found a mechanism *via* which the Ga atoms of $\text{Mo}_2\text{Ga}_2\text{C}$ can sequentially be replaced by O ones, we investigated the relative stability of the ABC- and ABA-stacked $\text{Mo}_2\text{Ga}_2\text{C}$ MAX phase models with varying O_{Ga} content. To this end, we used the total energies of optimized models that contain $2 \times 2 \times 1$ unit cells of $\text{Mo}_2\text{Ga}_2\text{C}$, in which different numbers of pairs of Ga atoms have been replaced by pairs of O atoms. Each unit cell contains two Ga–Ga pairs, allowing us to assess seven O concentrations between 0% ($\text{Mo}_2\text{Ga}_2\text{C}$) and 100% ($\text{Mo}_2\text{O}_2\text{C}$). As mentioned in the section with the computational methods, three approaches were considered separately: one without D3 dispersion corrections and a fixed supercell size, another with D3 corrections and fixed supercell size, and a final one including D3 corrections and optimizing the supercell size for each O concentration. The third of these methods is expected to yield the most reliable results, because we have

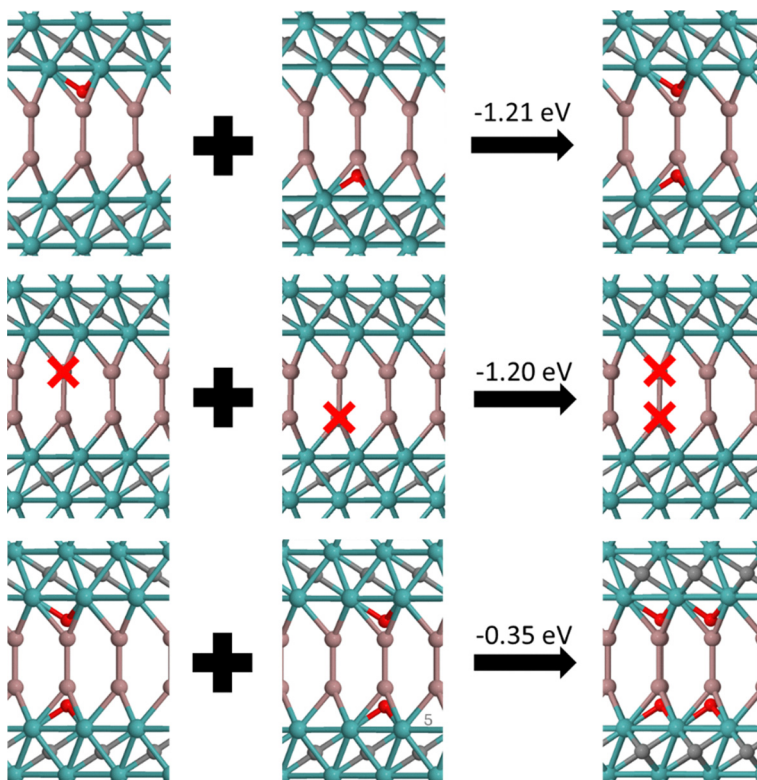


Fig. 5 Illustration of the attraction between single substitutional O atoms (top panels), single Ga vacancies (middle panels), and pairs of substitutional O atoms (bottom panels) in $\text{Mo}_2\text{Ga}_2\text{C}$. Colour code for the spheres: Mo in cyan, Ga in pink, C in grey, O in red. The red crosses denote Ga vacancies.

determined that $\text{Mo}_2\text{O}_2\text{C}$ is a van der Waals solid and because the lattice parameters should need to adapt to the replacement of Ga atoms by O ones.

The comparison of the relative stability of the ABC and ABA phases of the $\text{Mo}_2\text{Ga}_{2-x}\text{O}_x\text{C}$ models can be made with the aid of

Fig. 6. In this Figure, we find that the data obtained using all three methods described in the previous paragraph are nearly coincident, which suggests that van der Waals interactions have only a small effect on the lattice constants. In the $\text{Mo}_2\text{Ga}_2\text{C}$ MAX phase, the ABC atomic layer stacking is more

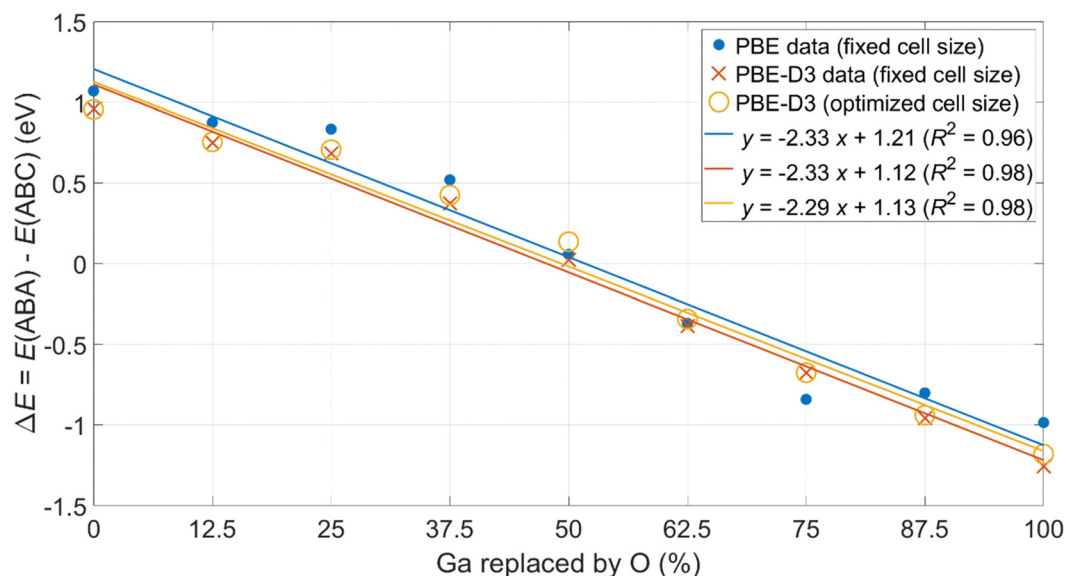


Fig. 6 Energetic difference per unit cell (ΔE) between the $\text{Mo}_2\text{Ga}_2\text{C}$ MAX phase with ABA and ABC atomic layer stacking, as a function of the percentage of Ga atoms that are replaced by O ones: 0 corresponds to the pristine $\text{Mo}_2\text{Ga}_2\text{C}$ MAX phase, 100 to the $\text{Mo}_2\text{O}_2\text{C}$ MOX phase, and values between 0 and 100 to intermediate O/Ga content.



stable than the ABA one by just over 1 eV, whereas if all the Ga content is replaced by O, this difference is reversed, with the ABA alignment being preferred by just over 1 eV. The results generate approximately symmetric linear relations around 50% replacement of Ga by O, the point near which the phase transition occurs.

Summary and conclusions

In this work, we employed density-functional theory (DFT) calculations using the PBE exchange–correlation functional, both with and without D3 dispersion corrections, as implemented in the VASP code, to investigate the transformation of the $\text{Mo}_2\text{Ga}_2\text{C}$ MAX phase into the Mo_2C MXene. Our results provide thermodynamic and structural insights into the etching process of Ga and subsequent surface functionalization by O atoms, with a focus on the evolution of atomic stacking sequences and defect energetics.

We found that the pristine $\text{Mo}_2\text{Ga}_2\text{C}$ MAX phase exhibits an ABC stacking of its atomic layers, in agreement with experimental data and previous theoretical work. As Ga atoms are progressively replaced by oxygen, the ABA stacking becomes increasingly favourable, with a crossover in stability occurring near 50% Ga-to-O substitution. This concentration marks a critical point for the phase transition from the ABC to the ABA configuration, which is energetically preferred for the resulting Mo_2CO_2 MXene by more than 1 eV per unit cell. The O substitution leads to a contraction of the lattice, as expected due to the smaller atomic size of oxygen compared to gallium. The calculated binding energies between the interacting Mo_2CO_2 MXene sheets are of about 0.2 eV per formula unit, which suggests a classification as a van der Waals solid of the material derived from the pristine $\text{Mo}_2\text{Ga}_2\text{C}$ MAX phase upon full Ga-to-O substitution. The results suggest that transformation from the ABA MAX phase to the MXene phase is thermodynamically favorable but, the replacement of Ga by O is expected to involve an energy barrier, as it requires chemical transformation and likely the breaking and formation of bonds.

By evaluating the formation energies of O and F atoms placed at three types of defect sites, namely, interstitial, Ga-substituted, and C-substituted, we found the stability to follow the order: Ga-substituted > interstitial > C-substituted, for both elements. Fluorine was consistently less thermodynamically favourable than oxygen. Notably, when replacing Ga, it was found that oxygen atoms occupy sites analogous to the FCC hollow positions typically favoured by surface terminations in MXenes, whereas fluorine atoms preferentially bond with remaining Ga atoms. This suggests the formation of incipient gallium fluoride species during the etching process, aligning with experimental findings for the Ti_3AlC_2 MAX phase, where Al is removed in the form of AlF_3 . Furthermore, the energetic analysis reveals that oxygen substitutions are more stable when occupying adjacent Ga–Ga pairs, indicating a cooperative or cascading mechanism during etching. These results support a defect-driven structural transition, in which O atoms

preferentially and locally replace Ga, thereby stabilizing neighbouring sites for subsequent substitution and promoting the progression of the Ga etching process.

Overall, our calculations shed light on the atomistic mechanisms driving the transformation of $\text{Mo}_2\text{Ga}_2\text{C}$ into the Mo_2C MXene under HF-based etching conditions, offering a theoretical explanation for the experimentally observed predominance of oxygen terminations and the associated structural shift from ABC to ABA stacking. The close agreement between our results and experimental findings strengthens the mechanistic understanding of this MXene synthesis pathway. Building on this foundation, further computational studies may help design alternative etching strategies that promote targeted surface terminations or stacking arrangements, potentially enabling the synthesis of MXenes that have so far remained experimentally elusive.

Conflicts of interest

There are no conflicts of interest to declare. The authors declare no competing interests.

Data availability

The data supporting this article have been included as part of the SI, which includes a representation of the structure of O_{Ga} in Mo_2GaC , and coordinates of optimized $2 \times 2 \times 1$ supercells of $\text{Mo}_2\text{Ga}_2\text{C}$ and $\text{Mo}_2\text{O}_2\text{C}$, either with ABC or ABA atomic layer stacking. See DOI: <https://doi.org/10.1039/d5cp02315g>

Acknowledgements

This work was developed within the scope of the projects CICECO-Aveiro Institute of Materials, with ref. UIDB/50011/2020, UIDP/50011/2020 and LA/P/0006/2020, HydroFormX with ref. 2023.12765.PEX, and CRF – CRG 2022 KAUST with ref. ORFS-2022-CRG11-5075.2. We are also thankful to FCT I. P. for the computational resources granted in the framework of project ref. 2024.13633.CPCA.A3 by the FCT 2024 Call for Advanced Computing Projects. JDG thanks the Portuguese Foundation for Science and Technology (FCT) through the grant with ref. 2023.06511.CEECIND, in the scope of the Individual Call to Scientific Employment Stimulus – 6th Edition.

References

- 1 M. Dahlqvist, M. W. Barsoum and J. Rosen, MAX phases – Past, present, and future, *Mater. Today*, 2024, **72**, 1–24, DOI: [10.1016/j.mattod.2023.11.010](https://doi.org/10.1016/j.mattod.2023.11.010).
- 2 M. Naguib, M. Kurtoglu, V. Presser, J. Lu, J. Niu, M. Heon, L. Hultman, Y. Gogotsi and M. W. Barsoum, Two-Dimensional Nanocrystals Produced by Exfoliation of Ti_3AlC_2 , *Adv. Mater.*, 2011, **23**, 4248–4253, DOI: [10.1002/adma.201102306](https://doi.org/10.1002/adma.201102306).



3 M. Rahman and M. S. Al Mamun, Future prospects of MXenes: synthesis, functionalization, properties, and application in field effect transistors, *Nanoscale Adv.*, 2024, **6**, 367–385, DOI: [10.1039/D3NA00874F](https://doi.org/10.1039/D3NA00874F).

4 H. Rohde and V. H. Kudielka, Strukturuntersuchungen an carbosulfiden von titan und zirkon, *Z. Krist.*, 1960, **114**, 447, DOI: [10.1524/zkri.1960.114.16.447](https://doi.org/10.1524/zkri.1960.114.16.447).

5 J. D. Gouveia, G. Novell-Leruth, P. M. L. S. Reis, F. Viñes, F. Illas and J. R. B. Gomes, First-Principles Calculations on the Adsorption Behavior of Amino Acids on a Titanium Carbide MXene, *ACS Appl. Bio Mater.*, 2020, **3**, 5913–5921, DOI: [10.1021/acsabm.0c00621](https://doi.org/10.1021/acsabm.0c00621).

6 J. D. Gouveia, G. Novell-Leruth, F. Viñes, F. Illas and J. R. B. Gomes, The Ti_2CO_2 MXene as a nucleobase 2D sensor: a first-principles study, *Appl. Surf. Sci.*, 2021, **544**, 148946, DOI: [10.1016/j.apsusc.2021.148946](https://doi.org/10.1016/j.apsusc.2021.148946).

7 J. D. Gouveia and J. R. B. Gomes, Adsorption of Hexoses on the Ti_2CO_2 MXene, *J. Phys. Chem. C*, 2024, **128**, 20369–20377, DOI: [10.1021/acs.jpcc.4c04821](https://doi.org/10.1021/acs.jpcc.4c04821).

8 J. D. Gouveia and J. R. B. Gomes, Effect of the surface termination on the adsorption of flue gas by the titanium carbide MXene, *Mater. Today Chem.*, 2023, **29**, 101441, DOI: [10.1016/j.mtchem.2023.101441](https://doi.org/10.1016/j.mtchem.2023.101441).

9 J. D. Gouveia, H. Rocha and J. R. B. Gomes, MXene-supported transition metal single-atom catalysts for nitrogen dissociation, *Mol. Catal.*, 2023, **547**, 113373, DOI: [10.1016/j.mcat.2023.113373](https://doi.org/10.1016/j.mcat.2023.113373).

10 J. D. Gouveia, Á. Morales-García, F. Viñes, J. R. B. Gomes and F. Illas, Facile Heterogeneously Catalyzed Nitrogen Fixation by MXenes, *ACS Catal.*, 2020, **10**, 5049–5056, DOI: [10.1021/acscatal.0c00935](https://doi.org/10.1021/acscatal.0c00935).

11 J. D. Gouveia, Á. Morales-García, F. Viñes, F. Illas and J. R. B. Gomes, MXenes as promising catalysts for water dissociation, *Appl. Catal., B*, 2020, **260**, 118191, DOI: [10.1016/j.apcatb.2019.118191](https://doi.org/10.1016/j.apcatb.2019.118191).

12 J. D. Gouveia and J. R. B. Gomes, The determining role of T_x species in the catalytic potential of MXenes: water adsorption and dissociation on Mo_2CT_x , *Catal. Today*, 2023, **424**, 113848, DOI: [10.1016/j.cattod.2022.07.016](https://doi.org/10.1016/j.cattod.2022.07.016).

13 S. Saharan, U. Ghanekar and S. Meena, V_2N MXene for Hydrogen Storage: First-Principles Calculations, *J. Phys. Chem. C*, 2024, **128**, 1612–1620, DOI: [10.1021/acs.jpcc.3c07786](https://doi.org/10.1021/acs.jpcc.3c07786).

14 T. Thomas, S. Bontha, A. Bishnoi and P. Sharma, MXene as a hydrogen storage material? A review from fundamentals to practical applications, *J. Energy Storage*, 2024, **88**, 111493, DOI: [10.1016/j.est.2024.111493](https://doi.org/10.1016/j.est.2024.111493).

15 P. Kumar, S. Singh, S. A. R. Hashmi and K.-H. Kim, MXenes: emerging 2D materials for hydrogen storage, *Nano Energy*, 2021, **85**, 105989, DOI: [10.1016/j.nanoen.2021.105989](https://doi.org/10.1016/j.nanoen.2021.105989).

16 N. Li, J. Peng, W.-J. Ong, T. Ma, Arramel, P. Zhang, J. Jiang, X. Yuan and C. (John) Zhang, MXenes: An Emerging Platform for Wearable Electronics and Looking Beyond, *Matter*, 2021, **4**, 377–407, DOI: [10.1016/j.matt.2020.10.024](https://doi.org/10.1016/j.matt.2020.10.024).

17 D. Ayodhya, A review of recent progress in 2D MXenes: synthesis, properties, and applications, *Diamond Relat. Mater.*, 2023, **132**, 109634, DOI: [10.1016/j.diamond.2022.109634](https://doi.org/10.1016/j.diamond.2022.109634).

18 D. Dhamodharan, M. A. Al-Harthi, B. Ramya, A. Bafaqueer and F. Alam, MXenes: a promising material with multi-functional applications, *J. Environ. Chem. Eng.*, 2024, **12**, 112316, DOI: [10.1016/j.jece.2024.112316](https://doi.org/10.1016/j.jece.2024.112316).

19 H. Kim and H. N. Alshareef, MXtronics: MXene-Enabled Electronic and Photonic Devices, *ACS Mater. Lett.*, 2020, **2**, 55–70, DOI: [10.1021/acsmaterialslett.9b00419](https://doi.org/10.1021/acsmaterialslett.9b00419).

20 L. E. Toth, High superconducting transition temperatures in the molybdenum carbide family of compounds, *J. Less Common Met.*, 1967, **13**, 129–131, DOI: [10.1016/0022-5088\(67\)90055-0](https://doi.org/10.1016/0022-5088(67)90055-0).

21 C. Hu, C.-C. Lai, Q. Tao, J. Lu, J. Halim, L. Sun, J. Zhang, J. Yang, B. Anasori, J. Wang, Y. Sakka, L. Hultman, P. Eklund, J. Rosen and M. W. Barsoum, Mo_2Ga_2C : a new ternary nanolaminated carbide, *Chem. Commun.*, 2015, **51**, 6560–6563, DOI: [10.1039/C5CC00980D](https://doi.org/10.1039/C5CC00980D).

22 R. Meshkian, L. Å. Näslund, J. Halim, J. Lu, M. W. Barsoum and J. Rosen, Synthesis of two-dimensional molybdenum carbide, Mo_2C , from the gallium based atomic laminate Mo_2Ga_2C , *Scr. Mater.*, 2015, **108**, 147–150, DOI: [10.1016/j.scriptamat.2015.07.003](https://doi.org/10.1016/j.scriptamat.2015.07.003).

23 Y. Guo, S. Jin, L. Wang, P. He, Q. Hu, L.-Z. Fan and A. Zhou, Synthesis of two-dimensional carbide Mo_2CT_x MXene by hydrothermal etching with fluorides and its thermal stability, *Ceram. Int.*, 2020, **46**, 19550–19556, DOI: [10.1016/j.ceramint.2020.05.008](https://doi.org/10.1016/j.ceramint.2020.05.008).

24 M. A. Hadi, New ternary nanolaminated carbide Mo_2Ga_2C : a first-principles comparison with the MAX phase counterpart Mo_2GaC , *Comput. Mater. Sci.*, 2016, **117**, 422–427, DOI: [10.1016/j.commatsci.2016.02.018](https://doi.org/10.1016/j.commatsci.2016.02.018).

25 C.-C. Lai, R. Meshkian, M. Dahlqvist, J. Lu, L. Å. Näslund, O. Rivin, E. N. Caspi, O. Ozeri, L. Hultman, P. Eklund, M. W. Barsoum and J. Rosen, Structural and chemical determination of the new nanolaminated carbide Mo_2Ga_2C from first principles and materials analysis, *Acta Mater.*, 2015, **99**, 157–164, DOI: [10.1016/j.actamat.2015.07.063](https://doi.org/10.1016/j.actamat.2015.07.063).

26 J. D. Gouveia, F. Viñes, F. Illas and J. R. B. Gomes, MXenes atomic layer stacking phase transitions and their chemical activity consequences, *Phys. Rev. Mater.*, 2020, **4**, 054003, DOI: [10.1103/PhysRevMaterials.4.054003](https://doi.org/10.1103/PhysRevMaterials.4.054003).

27 E. B. Deeva, A. Kurlov, P. M. Abdala, D. Lebedev, S. M. Kim, C. P. Gordon, A. Tsoukalou, A. Fedorov and C. R. Müller, In Situ XANES/XRD Study of the Structural Stability of Two-Dimensional Molybdenum Carbide Mo_2CT_x : Implications for the Catalytic Activity in the Water–Gas Shift Reaction, *Chem. Mater.*, 2019, **31**, 4505–4513, DOI: [10.1021/acs.chemmater.9b01105](https://doi.org/10.1021/acs.chemmater.9b01105).

28 G. Kresse and J. Furthmüller, Efficient iterative schemes for ab initio total-energy calculations using a plane-wave basis set, *Phys. Rev. B: Condens. Matter Mater. Phys.*, 1996, **54**, 11169–11186, DOI: [10.1103/PhysRevB.54.11169](https://doi.org/10.1103/PhysRevB.54.11169).

29 J. P. Perdew, K. Burke and M. Ernzerhof, Generalized Gradient Approximation Made Simple, *Phys. Rev. Lett.*, 1996, **77**, 3865–3868, DOI: [10.1103/PhysRevLett.77.3865](https://doi.org/10.1103/PhysRevLett.77.3865).



30 P. E. Blöchl, Projector augmented-wave method, *Phys. Rev. B: Condens. Matter Mater. Phys.*, 1994, **50**, 17953–17979, DOI: [10.1103/PhysRevB.50.17953](https://doi.org/10.1103/PhysRevB.50.17953).

31 S. Grimme, J. Antony, S. Ehrlich and H. Krieg, A consistent and accurate ab initio parametrization of density functional dispersion correction (DFT-D) for the 94 elements H–Pu, *J. Chem. Phys.*, 2010, **132**, 154104, DOI: [10.1063/1.3382344](https://doi.org/10.1063/1.3382344).

32 J. D. Gouveia, T. L. P. Galvão, K. Iben Nassar and J. R. B. Gomes, First-principles and machine-learning approaches for interpreting and predicting the properties of MXenes, *npj 2D Mater. Appl.*, 2025, **9**, 8, DOI: [10.1038/s41699-025-00529-5](https://doi.org/10.1038/s41699-025-00529-5).

33 A. S. Tygesen, M. Pandey, T. Vegge, K. S. Thygesen and J. M. García-Lastra, Role of Long-Range Dispersion Forces in Modeling of MXenes as Battery Electrode Materials, *J. Phys. Chem. C*, 2019, **123**, 4064–4071, DOI: [10.1021/acs.jpcc.8b11663](https://doi.org/10.1021/acs.jpcc.8b11663).

34 J. Liu, T. Shen, J.-C. Ren, S. Li and W. Liu, Role of van der Waals interactions on the binding energies of 2D transition-metal dichalcogenides, *Appl. Surf. Sci.*, 2023, **608**, 155163, DOI: [10.1016/j.apsusc.2022.155163](https://doi.org/10.1016/j.apsusc.2022.155163).

35 H. J. Monkhorst and J. D. Pack, Special points for Brillouin-zone integrations, *Phys. Rev. B: Condens. Matter Mater. Phys.*, 1976, **13**, 5188–5192, DOI: [10.1103/PhysRevB.13.5188](https://doi.org/10.1103/PhysRevB.13.5188).

36 M. Nadeem, M. Haseeb, A. Hussain, A. Javed, M. A. Rafiq, M. Ramzan, M. N. Rasul and M. A. Khan, Structural stability, electronic structure, mechanical and optical properties of MAX phase ternary $\text{Mo}_2\text{Ga}_2\text{C}$, Mo_2GaC and Mo_3GaC_2 carbides, *J. Mater. Res. Technol.*, 2021, **14**, 521–532, DOI: [10.1016/j.jmrt.2021.06.079](https://doi.org/10.1016/j.jmrt.2021.06.079).

37 B. Anasori, M. R. Lukatskaya and Y. Gogotsi, 2D metal carbides and nitrides (MXenes) for energy storage, *Nat. Rev. Mater.*, 2017, **2**, 16098, DOI: [10.1038/natrevmats.2016.98](https://doi.org/10.1038/natrevmats.2016.98).

38 P. P. Michałowski, M. Anayee, T. S. Mathis, S. Kozdra, A. Wójcik, K. Hantanasirisakul, I. Jóźwik, A. Piątkowska, M. Moźdzonek, A. Malinowska, R. Diduszko, E. Wierzbicka and Y. Gogotsi, Oxy carbide MXenes and MAX phases identification using monoatomic layer-by-layer analysis with ultralow-energy secondary-ion mass spectrometry, *Nat. Nanotechnol.*, 2022, **17**, 1192–1197, DOI: [10.1038/s41565-022-01214-0](https://doi.org/10.1038/s41565-022-01214-0).

39 P. P. Michałowski, Unraveling the composition of each atomic layer in the MXene/MAX phase structure – identification of oxy carbide, oxynitride, and oxy carbonitride subfamilies of MXenes, *Nanoscale Horiz.*, 2024, **9**, 1493–1497, DOI: [10.1039/D4NH00151F](https://doi.org/10.1039/D4NH00151F).

40 J. D. Gouveia and J. R. B. Gomes, Structural and electronic properties of the titanium carbide MXene with variable sublattice oxygen composition, *Surf. Interfaces*, 2024, **46**, 103920, DOI: [10.1016/j.surfin.2024.103920](https://doi.org/10.1016/j.surfin.2024.103920).

41 J. D. Gouveia and J. R. B. Gomes, Effect of surface composition on the stability of Ti- and V-based oxy carbide and oxynitride MXenes, *Mater. Today Phys.*, 2024, **46**, 101481, DOI: [10.1016/j.mtphys.2024.101481](https://doi.org/10.1016/j.mtphys.2024.101481).

42 J. Z. Duan, J. R. Zhang, C. L. Wang, Y. Qiu, W. S. Duan and L. Yang, First principles investigation of point defect-related properties in Ti_2AlN , *RSC Adv.*, 2014, **4**, 42014–42021, DOI: [10.1039/C4RA07200F](https://doi.org/10.1039/C4RA07200F).

43 F. Colonna and C. Elsässer, First principles DFT study of interstitial hydrogen and oxygen atoms in the MAX phase Ti_2AlN , *RSC Adv.*, 2017, **7**, 37852–37857, DOI: [10.1039/C7RA05045C](https://doi.org/10.1039/C7RA05045C).

44 J. D. Gouveia and J. R. B. Gomes, Structural and energetic properties of vacancy defects in MXene surfaces, *Phys. Rev. Mater.*, 2022, **6**, 024004, DOI: [10.1103/PhysRevMaterials.6.024004](https://doi.org/10.1103/PhysRevMaterials.6.024004).

45 J. Björk and J. Rosen, Functionalizing MXenes by Tailoring Surface Terminations in Different Chemical Environments, *Chem. Mater.*, 2021, **33**, 9108–9118, DOI: [10.1021/acs.chemmater.1c01264](https://doi.org/10.1021/acs.chemmater.1c01264).